Equilibrium and Kinetic Folding of Pigeon Lysozyme†

P. Haezebrouck, K. Noyelle, and H. Van Dael*

Interdisciplinary Research Center, Katholieke Universiteit Leuven, Campus Kortrijk, B-8500 Kortrijk, Belgium

Received December 17, 1997; Revised Manuscript Received February 23, 1998

ABSTRACT: In the present study, the search for a possible intermediate state in pigeon lysozyme is addressed by equilibrium and kinetic experiments using static and stopped-flow fluorescence and circular dichroism spectroscopies. In equilibrium conditions at pH 7.5, pigeon lysozyme shows no populated intermediate state in temperature- and GdnHCl-induced unfolding experiments. In the unfolding process at low pH, however, a distinct intermediate state with molten globule characteristics is observed. Ca^{2+} binding to the protein is found to stabilize the native state. The early folding intermediate observed in kinetic experiments corresponds to the equilibrium intermediate in that an important amount of secondary structure has already been established. Full accomplishment of native tertiary contacts is achieved in a fast exponential process with a rate constant (0.23−135 s^{-1}) that is strongly dependent on refolding conditions. Binding experiments with the fluorescent inhibitor MeU-diNAG support these conclusions. The folding rate is not influenced by Ca^{2+} binding. Analysis of the refolding and unfolding kinetics determined as a function of denaturant concentration leads to a Gibbs energy profile with a rate-determining transition state between the N- and I-states. Comparison with previous results on the folding of hen egg white lysozyme emphasizes the crucial role of Trp 62 in stabilizing non-native interactions. The replacement of this residue by Tyr in pigeon lysozyme contributes to the formation of native tertiary contacts.

The mechanism by which an unfolded polypeptide chain acquires a specific, densely packed, and cooperative three-dimensional structure remains one of the major unsolved questions of molecular biology. A major goal of experimental work on trying to unravel this mechanism is to detect and characterize partially folded states, including transient intermediates observed in kinetic experiments, and stable intermediates occurring under equilibrium conditions. As some of the kinetic intermediates resemble equilibrium molten globules, the idea has grown that partially folded intermediates could be of general importance in directing a protein toward the native state (*1*−*4*). Whether these intermediates are productive and required for further folding or whether they merely accumulate prior to a slow step of folding is, however, not clear. Kinetic traps and high-energy barriers could occur if non-native interactions are stabilized in these structures (*5*−*7*). In this regard, it is particularly interesting to look for possible intermediates in fast folding proteins and to determine the nature of the rate-limiting step in the folding process. The existence of such intermediates can be inferred from the effect of denaturants on the kinetics of folding. A simple two-state folding and unfolding transition is characterized by a V-shaped behavior of the logarithm of the observed rates versus denaturant concentration. Various proteins exhibit this two-state behavior only in the transition region and deviate markedly at low denaturant concentration where the observed rate of folding levels off. Such a behavior is generally accepted to be a criterion for the existence of an intermediate state (*8*−*10*).

In this work, we have analyzed the equilibrium and kinetic intermediate states of pigeon lysozyme with equilibrium and stopped-flow fluorescence and circular dichroism (CD)[1] techniques. An analysis of the refolding and unfolding rates as a function of GdnHCl concentration has led to a free-energy diagram of the folding transition including the energy levels of the intermediate and transition states. Comparison with the kinetics of other lysozymes has thrown light on the role of Trp 62 in stabilizing non-native interactions during the refolding process of hen egg white lysozyme.

Pigeon egg white lysozyme is a *c*-type lysozyme consisting of a single polypeptide chain with 127 amino acid residues and with a molecular mass of about 14 517 Da. Its sequence was found to be identical with that of hen egg white lysozyme at 61 equivalent positions including those of the catalytic residues Glu 53 and Asp 52 (*11*). Pigeon lysozyme, however, differs from the other *c*-type lysozymes in that it binds Ca^{2+} ions tightly (*12*). In this respect, it is more similar to α-lactalbumin, an evolutionary and structurally related protein but with a totally different enzymatic role. Like in all α-lactalbumins, binding of Ca^{2+} provokes a significant stabilization in pigeon lysozyme (*12*). The X-ray structure analysis of pigeon lysozyme showed that its main-chain folding is similar to that of chicken lysozyme. The largest differences between both structures are situated in the surface loop regions which connect secondary structural units (*13*, *14*). Stability and unfolding studies of pigeon lysozyme have

† This work is supported by funds of the Flemish F. W. O. and K. U. Leuven Research Council. P.H. is a K. U. Leuven Postdoctoral fellow.

* To whom correspondence should be addressed. Fax: +32-56-246997. Telephone: +32-56-246111. E-mail: Herman.VanDael@kulak.ac.be.

[1] Abbreviations: bis-ANS, 4, 4′-bis[1-(phenylamino)-8-naphthalenesulfonate]; CD, circular dichroism; GdnHCl, guanidine hydrochloride; MeU-diNAG, 4-methylumbelliferyl-*N*,*N*′-diacetyl-β-chitobiose.

S0006-2960(97)03105-X CCC: $15.00
Published on Web 04/18/1998

been scarcely documented and to our knowledge are limited to the stationary CD-monitored unfolding curves in the presence of various GdnHCl concentrations (*15*). The latter results indicate that at neutral pH the apo as well as the Ca^{2+}-bound forms of pigeon lysozyme unfold by a two-state mechanism without the appearance of an observable intermediate state. They contrast with the well-documented observations of an intermediate state with molten globule characteristics (*16*−*18*) in apo equine lysozyme which, like the pigeon variant, has the Ca^{2+}-binding capacity. A related matter of concern in our study is whether such an intermediate state could exist under other conditions especially at acid pH as found for human and hen lysozyme (*19, 20*).

MATERIALS AND METHODS

Pigeon Lysozyme. Pigeon lysozyme was prepared from the egg white of new-laid pigeon eggs obtained from the breeding station "Natural" (Zoersel, Belgium). The sample was prepared for chromatography by adding 1 volume of 1 M potassium phosphate buffer, pH 6.9, to 9 volumes of egg white to give a final buffer concentration of 0.1 M. The solution was stirred for 30 min. Undissolved mucous remainders and phospholipids from the yolk were removed by centrifugation at 7500*g* for 15 min at 4 °C.

In the first purification step, the fluidized bed technology, using the Streamline system, was exploited (*21*). The clear supernatant was diluted 10 times to obtain a final buffer concentration of 20 mM. The Streamline-SP adsorbent gel was fluidized in a Streamline C-50 column using 20 mM potassium phosphate, 0.02% NaN_3, pH 6.9, as equilibration buffer. Subsequently, the diluted pigeon egg white was pumped into the column and the gel washed with equilibration buffer until the nonbound proteins were removed. The gel beads were allowed to sediment, the adaptor was lowered, and the adsorbed proteins were eluted in a downward direction using the equilibrium buffer with 2 M NaCl. The salt fraction, which displayed lytic activity on *Micrococcus* cell walls, was dialyzed against water and lyophylized. Second, the sample was subjected to size-exclusion chromatography on a Sephacryl HR-100 (Pharmacia) column, using 50 mM NaOAc, 0.2 M NaCl, 0.02% NaN_3, pH 5.0. Finally, the lytic fraction was loaded onto a cation-exchange column, Fractogel-EMD-SO_3- (Merck), equilibrated with 25 mM Tris, pH 8.0. Pigeon lysozyme was eluted with a linear NaCl gradient (0−2 M). The final yield was around 30 mg/L of egg white.

The purity of the product was controlled by isoelectric focusing on precoated plates (Serva). The near-UV CD spectrum was identical with the one described in the literature (*22*). As the pure lysozyme contained at least 1 mol of Ca^{2+}/mol of protein, EDTA was added to the buffer in order to remove Ca^{2+} ions for studies of the apo form.

Equilibrium Circular Dichroism Experiments. Circular dichroism measurements were carried out on a Jasco J-600A spectropolarimeter using cuvettes of 1 cm path length in the near-UV and 1 mm in the far-UV region. The data were expressed as residual ellipticity, $[\theta]$ (deg·cm^2 dmol^{-1}), using 114.3 as the mean residue weight for pigeon lysozyme. Protein concentration was about 0.35 mg/mL. The temperature was kept constant by circulating thermostated water through the cell holder and was measured with a calibrated thermocouple. The instrument was regularly calibrated with a 1 mg/mL solution of 10-camphorsulfonic acid.

Stopped-Flow Fluorescence Measurements. Fluorescence-detected refolding and unfolding experiments were performed on a SX.17 MV sequential mixing stopped-flow spectrometer from Applied Photophysics (Leatherhead, U.K.). The stopped-flow module and the observation cell with 2 mm path length were thermostated by circulating water from a temperature-controlled water bath. A double monochromator was used for excitation at 280 nm, and the fluorescence emission was measured using a high-pass filter with a 320 nm cutoff. The dead-time of the instrument was estimated to be about 2 ms. Typically, kinetics were measured 10−20 times under identical conditions, averaged, and analyzed as mono- or biexponential functions by using the manufacturer's software.

For refolding experiments, a solution of unfolded pigeon lysozyme in 6 M GdnHCl and the appropriate buffer was diluted 11-fold with refolding buffer, containing different amounts of GdnHCl, to yield final concentrations ranging from 0.54 to 4 M and a final protein concentration of 25 μM. To initiate unfolding, 270 μM native lysozyme in buffer was diluted 11-fold with GdnHCl solutions of varying concentrations to give final denaturant concentrations between 3 and 6 M. In each kinetic experiment, the base lines corresponding to the intial and final states were recorded in order to fix the global fluorescence intensity at these states and to check for possible mixing artifacts. Pure GdnHCl was purchased from Merck. As GdnHCl is hygroscopic, the exact concentration was determined from refractive index measurements (*23*).

Binding of MeU-diNAG. 4-Methylumbelliferyl-*N*,*N*′-diacetyl-β-chitobiose is a fluorescent inhibitor purchased from Sigma. Using an excitation wavelength of 330 nm, the total fluorescence emission above 335 nm was monitored. The protein solution (9.7 mg/mL) in 6 M GdnHCl was diluted 11-fold with a solution of 20 mM MES, 80 mM NaCl, 2 mM Ca^{2+}, pH 6, containing 6 μM MeU-diNAG. The base line representative for the unbounded probe was acquired by diluting 6 M GdnHCl in the absence of protein with 10 volumes of the refolding buffer containing 6 μM MeU-diNAG.

Stopped-Flow CD Measurements. Stopped-flow CD was performed with the SX.17 MV stopped-flow reaction analyzer equipped with a CD detector from Applied Photophysics. The dead-time of the instrument in the CD mode is 8 ms for an observation chamber of 2 mm optical path length. Kinetics were determined from CD signals at 225 nm. Each kinetic record is the signal-average of at least 20 measurements. Refolding was typically followed for up to 2 s, using at the most 2000 data points.

RESULTS

Thermal Unfolding. Figure 1 shows the thermal unfolding of apo-pigeon lysozyme at pH 4.5, monitored by circular dichroism spectroscopy at 276 nm in the near-UV region and at 222 nm in the far-UV region. The transitions in both wavelength regions coincide completely, indicating that tertiary and secondary structures of the protein unfold simultaneously in a cooperative process. T_m, the temperature denoting the midpoint of the transition curve, equals 63 °C for the apo-protein and 76 °C upon the addition of 10 mM

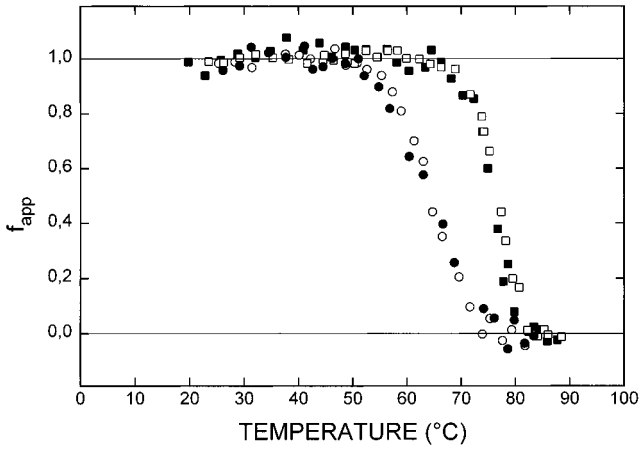

FIGURE 1: Thermal unfolding of pigeon lysozyme at pH 4.5, monitored at 276 nm (open symbols) and 222 nm (filled symbols). The apparent fraction of folded protein has been plotted against temperature. Circles refer to data obtained in 10 mM NaOAc and 90 mM NaCl, squares to data obtained in the same buffer with 10 mM Ca^{2+}.

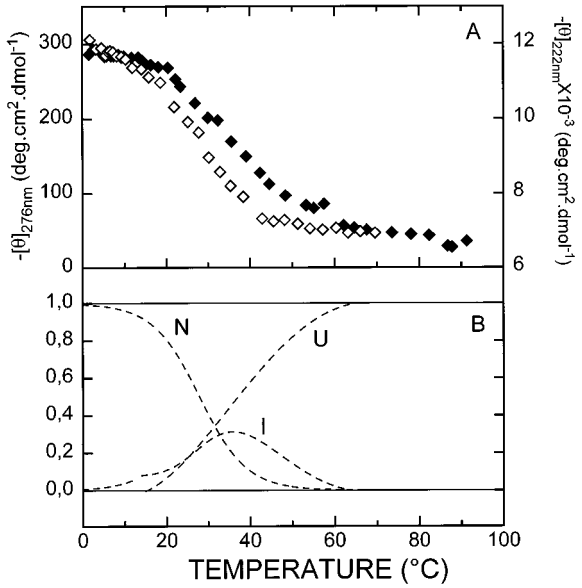

FIGURE 2: (A) Temperature dependence of the ellipticity of pigeon lysozyme at 276 nm (◇, left scale) and at 222 nm (◆, right scale) in acidic conditions, pH 1.0. (B) Temperature dependence of the population in the native (N), intermediate (I), and denatured states (U) at pH 1.0.

Ca^{2+}. At pH 4.5, the thermal unfolding of pigeon lysozyme therefore can be characterized as a two-state process, strongly stabilized by the binding of Ca^{2+} ions. These results are in complete agreement with earlier unfolding experiments induced by the addition of guanidine hydrochloride (*15*).

In acidic conditions (pH 1.0) the thermal unfolding curves obtained from the CD ellipticity in the near-UV and far-UV region no longer coincide (Figure 2A). The unfolding of the tertiary structure proceeds in the temperature range 10−45 °C with a T_m value of 28 °C. The unfolding of the secondary structure, on the other hand, is somewhat retarded. Starting from near 20 °C, the transition reaches the base level referring to the denatured state above 60 °C with a $T_m = 36$ °C. This result strongly suggests the occurrence of an equilibrium partially folded state. At 42 °C, for example, the ellipticity at 276 nm is indicative for the presence of exclusively nonspecific tertiary interactions or possibly for the total absence of tertiary structure. On the other hand, the ellipticity at 222 nm, observed at that temperature, shows the presence of about 30% of the secondary structure which has been found in the native state.

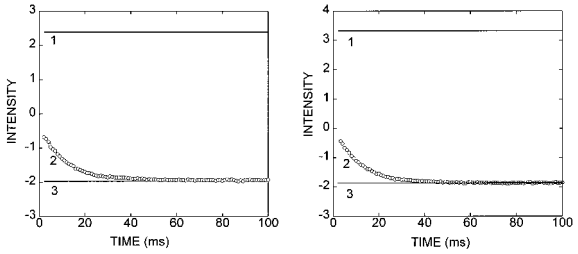

FIGURE 3: Time course of the refolding of pigeon lysozyme in 20 mM Tris, 80 mM NaCl, pH 7.5 at 25 °C, for the apo form (in 10 mM EDTA, left panel) and the Ca^{2+} form (in 10 mM Ca^{2+}, right panel). Refolding from a 6 M GdnHCl solution is induced by 11-fold dilution by the buffer solution, obtaining a final concentration of 0.54 M GdnHCl. Curve 1 indicates the equilibrium fluorescence of the unfolded state in 6 M GdnHCl, curve 2 gives the time-dependent evolution of the signal, and curve 3 indicates the equilibrium final state in 0.54 M GdnHCl.

From the normalized unfolding curves, the population in the native, intermediate and unfolded states can easily be calculated (*19, 24*). As becomes clear from Figure 2B, an intermediate state occurs between 10 and 60 °C with a maximum population of 31% at 36 °C. In previous unfolding studies (*15*), the unfolding transition of apo-pigeon lysozyme was characterized as two-state even at low pH and the intermediate state was never observed. Our present results agree with our previous observation of partially folded intermediate states in hen and human lysozyme at low pH (*19*) and with recent acid-induced unfolding studies of hen egg-white lysozyme (*20*).

Influence of Ca^{2+} on the Refolding Kinetics. The refolding kinetics of pigeon lysozyme are measured at pH 7.5, 25 °C, and shown in Figure 3. About 60% of the total fluorescence change occurs during the dead-time of the stopped-flow experiment. The remaining decrease in fluorescence can be described by a single-exponential function with a rate constant of 92 s^{-1} for the apo form as well as for the Ca^{2+} form. It is remarkable that the rates of fluorescence decrease for both forms are exactly the same. Although the stability of pigeon lysozyme is drastically affected by Ca^{2+} ions (*15*, this work), these ions do not induce a measurable effect on the rate of the refolding process. This contrasts to what is observed in the case of α-lactalbumin where the stability increase by Ca^{2+} ions is accompanied by a drastic gain in refolding rate (*25*). Our own observation of the refolding kinetics of α-lactalbumin in the same conditions as those used for pigeon lysozyme show a refolding rate of 0.04 s^{-1} for the apo form and 26 s^{-1} in the presence of 10 mM Ca^{2+} (Haezebrouck, Joniau, Noyelle, and Van Dael, unpublished results). Also Ca^{2+}-binding mutants of human lysozyme show a significant increase of the refolding rate upon Ca^{2+} binding (Haezebrouck, Joniau, Noyelle, and Van Dael, unpublished results).

Folding−Unfolding Kinetics. A detailed characterization of the folding and unfolding kinetics of pigeon lysozyme was performed by systematic stopped-flow fluorescence measurements as a function of GdnHCl concentration. The refolding kinetics at 25 °C, pH 6 (2 mM Ca^{2+}, 20 mM MES, 80 mM NaCl), following a rapid jump from 6 M to various

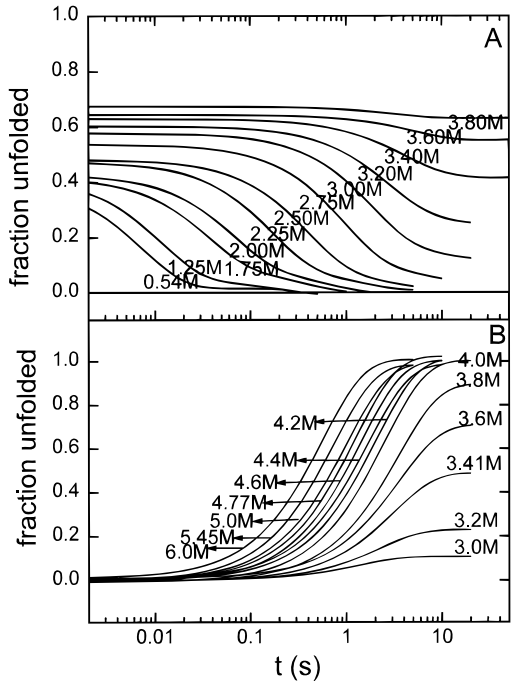

FIGURE 4: Fluorescence-detected kinetic traces of the refolding (A) and the unfolding (B) of pigeon lysozyme at pH 6 in 2 mM Ca^{2+}, 20 mM Mes, and 80 mM NaCl at 25 °C. For the refolding experiments, traces obtained at the indicated final GdnHCl concentration were normalized to the fluorescence intensity of the unfolded protein and the native protein. The fluorescence intensity in the unfolded state was constant (1.93 arbitrary units) but was slightly dependent on the GdnHCl concentration in the folded state ($-2.43 + 0.11$ [GdnHCl]). The curves shown in (A) are the result of a fit of the data points by a double exponential function.

final GdnHCl concentrations ranging from 4 to 0.54 M are shown in Figure 4A. Three different phases can be discerned in the refolding process. The first phase occurs during the dead-time of the instrument and is given by the difference between the fluorescence of the unfolded protein in 6 M GdnHCl and the initial fluorescence after the dead-time of mixing. The magnitude of this initial burst phase is strongly dependent on the final denaturant concentration. At 4 M GdnHCl, the concomitant fluorescence change corresponds to 30% of the total fluorescence change. When the final concentration of denaturant is lowered, this amount progressively increases and reaches 70% of the total change at 0.54 M (Figure 4A). A similar dependence of the unfolded fraction in the dead-time on the denaturant concentration has been found previously in ubiquitin (*26*) and cytochrome *c* (*3*) but was totally absent in a Trp-containing mutant of ribonuclease A (*27*). The kinetics of this initial burst phase could not be analyzed further. The subsequent decrease in fluorescence generally proceeds in a fast phase, representing about 80% of the remaining amplitude and a slow phase with an amplitude of 20%.

For each concentration of GdnHCl, the degree of refolding during the dead-time and the relative contribution of both phases in the refolding process are shown in Table 1. Only below 1 M and above 3.2 M GdnHCl the kinetic changes can be described by a monoexponential process covering practically the total amplitude. The rate of refolding is strongly dependent on the final denaturant concentration in that it decreases more than 500 times in the concentration range 0.54−4 M.

The unfolding kinetics following a jump from 0 M to final concentrations from 3 to 6 M GdnHCl can be described by a single exponential function (Figure 4B). Under unfolding conditions, the dead-time event becomes completely negligible. The effect of the final denaturant concentration is rather small as the rate constant changes maximally with a factor of 6 (Table 1). The lowest rate is obtained at a concentration of 3.4 M.

In Figure 5A, the apparent rate constant for the fast phase of refolding and unfolding at 25 °C is plotted on a logarithmic scale as a function of GdnHCl concentration. The V-shaped curve that shows the dependence of log k_{app} versus GdnHCl concentration, goes through a minimum near the midpoint of the corresponding equilibrium transition (Figure 5C).

Analysis of Equilibrium and Kinetic Unfolding. The GdnHCl-induced equilibrium unfolding of pigeon lysozyme (Figure 5C), measured in the same experimental conditions as the refolding−unfolding kinetics, has been analyzed using a two-state approximation (*28*, *29*):

$$N \leftrightarrow U \quad (1)$$

$$K_D = [U]/[N] \quad (2)$$

N and U represent the native and completely denatured state of pigeon lysozyme; K_D is the equilibrium unfolding constant. The equilibrium data have been fit according to the linear

Table 1: Refolding/Unfolding of Pigeon Lysozyme in 20 mM MES, 80 mM NaCl, 2 mM Ca^{2+}, pH 6.0 at 25 °C, followed by Stopped-Flow Fluorescence Spectroscopy

		fast phase refolding		slow phase refolding			
$[GdnHCl]_{end}$ (M)	refolding during dead-time (%)	rate (s^{-1})	amplitude (%)	rate (s^{-1})	amplitude (%)	$[GdnHCl]_{end}$ (M)	unfolding rate (s^{-1})
0.54	69.2	135	98.9	9.00	1.1	6.0	1.77
1.25	63.9	89.8	85.5	4.9	14.5	5.45	1.35
1.75	59.8	28.8	76.5	2.96	23.5	5.00	0.98
2.00	58.0	13.1	78.1	1.45	21.9	4.77	0.80
2.25	52.8	5.45	82.4	0.56	17.6	4.60	0.71
2.50	51.8	2.68	81.5	0.51	18.5	4.40	0.59
2.75	46.2	1.11	82.1	0.22	17.9	4.20	0.49
3.00	42.1	0.58	82.4	0.12	17.6	4.00	0.40
3.20	39.6	0.38	83.6	0.10	16.4	3.80	0.33
3.40	37.0	0.23	100	/	/	3.60	0.29
3.60	35.5	0.23	94.1	/	/	3.40	0.28
3.80	32.5	/	/	/	/	3.20	0.32
3.95	34.9	/	/	/	/	3.00	0.44
						2.80	0.76

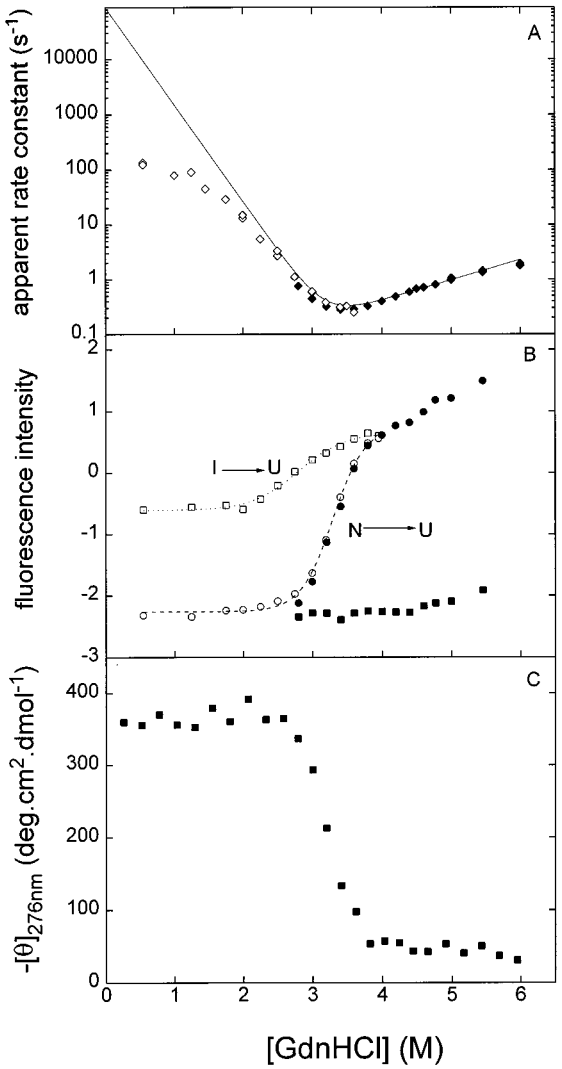

FIGURE 5: Dependence of the kinetics of unfolding (filled symbols) and refolding (open symbols) on the GdnHCl concentration. In (A), the apparent rate constants of unfolding (◆) and the fast phase of refolding (◇) are shown as a function of the final GdnHCl concentration. The solid curve is the result of calculations based on the two-state model. In (B), the initial (□, ■) and final (○, ●) values of the fluorescence intensity during refolding (open) and unfolding (filled) are shown. Sigmoidal fits based on the two-state model are represented by the dotted curve (I → U) and by the dashed curve (N → U). In (C), the equilibrium denaturation of pigeon lysozyme by GdnHCl at pH 6, 25 °C, in 20 mM MES, 80 mM NaCl is depicted. The midpoint of the transition lies at 3.2 M GdnHCl.

extrapolation model (*29*), assuming a linear dependence of ΔG_D on the GdnHCl concentration:

$$\Delta G_D = \Delta G_D(H_2O) + m_D[\text{GdnHCl}] \quad (3)$$

ΔG_D is the free energy of unfolding and $\Delta G_D(H_2O)$ is the free energy of unfolding in the absence of denaturant; m_D is a constant proportional to the increase in degree of exposure to solvent of the protein upon denaturation. As a result, the following values for $\Delta G_D(H_2O) = 39 \pm 1$ kJ mol^{-1} and $m_D = -12.1 \pm 0.5$ kJ mol^{-1} M^{-1} have been obtained. This value of the free energy of unfolding agrees well with the free energy difference between the native and unfolded states obtained from thermal denaturation experiments, $\Delta_N^U G = 40.5 \pm 3$ kJ mol^{-1}.

If the folding−unfolding kinetics are described by a simple two-state process, the apparent rate constant is equal to the sum of the microscopic rate constants of unfolding and refolding, k_{NU} and k_{UN}:

$$k_{app} = k_{NU} + k_{UN} \quad (4)$$

These rate constants depend linearly on denaturant concentration:

$$\log k_{NU} = \log k_{NU}(H_2O) + m_{NU}[\text{GdnHCl}] \quad (5)$$

$$\log k_{UN} = \log k_{UN}(H_2O) + m_{UN}[\text{GdnHCl}] \quad (6)$$

$k_{NU}(H_2O)$ and $k_{UN}(H_2O)$ are the microscopic rate constants for unfolding and refolding in the absence of denaturant.

The observed rate constants for the unfolding of pigeon lysozyme (Figure 5A, right side of the V-curve) increase with increasing GdnHCl concentration, conforming to eq 5 with $k_{NU}(H_2O) = 0.014 \pm 0.003$ s^{-1} and $m_{NU} = 0.37 \pm 0.02$ M^{-1}.

In the case of a simple two-state mechanism, log k_{UN} can be deduced from the m_{NU} value of the unfolding kinetics and from the equilibrium data (*8*):

$$\log k_{UN} = \log k_{UN}(H_2O) + (m_{NU} - m_D^*)[\text{GdnHCl}] \quad (7)$$

m_D^* is calculated from the equilibrium m_D value ($m_D^* = m_D/-2.3026RT$) and $k_{UN}(H_2O) = k_{NU}(H_2O)/k_D(H_2O)$ with $K_D(H_2O) = \exp[-\Delta G_D(H_2O)/RT]$. The solid curve in Figure 5A has been calculated for an ideal two-state system using the eqs 4, 5, and 7. Although very good agreement has been found in the fitting to experimental points at rather high denaturant concentrations, the refolding rates at low GdnHCl concentrations (<2 M) deviate considerably from the rates predicted by the two-state model. The nonlinear rate profile with decreasing slope at low denaturant concentration is classic evidence for the existence of a kinetic intermediate on the refolding pathway (*8*, *30*, *31*). The observed deviation from the two-state model is consistent with the fact that an important part of the fluorescence change accompanying the refolding process occurs during the dead-time (Figure 4A and Table 1).

The final values of the fluorescence on the unfolding−refolding kinetics diagram presented in Figure 5B show the N → U transition. This curve coincides with the equilibrium unfolding transition. On the other hand, the initial fluorescence intensities observed in the kinetic refolding process are a measure for the population of the burst-phase intermediate. Below 2 M, this population remains rather constant, but at higher concentrations a progressive destabilization of this state favors the occupation of the unfolded state. The upper curve of Figure 5B represents the I → U unfolding and shows that this unfolding process can be described as a two-state transition. In analogy with the equilibrium unfolding transition, it can be analyzed on the basis of a linear free energy relationship. The fitting indicates that the free energy difference between the kinetic intermediate and the U-state in the absence of GdnHCl, $\Delta G_{IU}(H_2O)$, equals 18.5 ± 7 kJ mol^{-1} and that the dependence of ΔG on the denaturant concentration m_{IU} amounts to -6.6 ± 0.2 kJ mol^{-1} M^{-1}.

As the unfolding of the kinetic intermediate only starts above 2 M GdnHCl, it is reasonable to assume that the observed rate constant below 2 M is that for the formation of the native state from the kinetic intermediate being accumulated in the burst phase. In the region from 0.54 to 2 M, the decrease in log k_{app} is linear, and the kinetics approach an apparent two-state behavior between I and N (*10*). By linear extrapolation <2 M GdnHCl, we have obtained $k_{IN}(H_2O) = 251 \pm 51\ s^{-1}$ and $m_{IN} = -0.4 \pm 0.1\ M^{-1}$.

Binding of MeU-diNAG to Refolding Pigeon Lysozyme. An important question remaining to be solved is whether the final state obtained at the end of the refolding process in 0.54 M GdnHCl corresponds to the active native enzyme. Binding of a competitive inhibitor during refolding provides a powerful way to determine directly the rate of appearance of the native state. In lysozyme, especially, the active site is situated at the interface between the two folding domains. The kinetics of its organization, therefore, provide insight into the process by which the two domains become integrated into a cooperative native structure. MeU-diNAG is a substrate analogue for which binding to the active site of lysozyme results in an increase of its fluorescence that can conveniently be monitored in a stopped-flow experiment in the absence of interference from the intrinsic fluorescence of the protein (*32*). This technique has already successfully been applied in kinetic studies of tertiary interactions during the refolding of hen lysozyme (*33*, *34*). These experiments also showed that the presence of the inhibitor did not affect the refolding kinetics of lysozyme itself. The binding of MeU-diNAG to native lysozyme proceeds in an exponential process, with a time constant of about 5 ms (*33*). In refolding experiments, therefore, the rates of any phases found to be slower than this must be limited by events in the folding process.

This type of experiment can also be used to reveal structural details of the early intermediate state observed on the folding pathway just after the dead-time of the apparatus. If during this burst phase no native contacts are established in the area of the active site, the inhibitor certainly will not bind and no major enhancement of the fluorescence intensity will be detected. If, on the other hand, the organization of native interactions in the domain interface has progressed to a level that enables binding of the probe, fluorescence will increase accordingly.

The time course of the binding of MeU-diNAG to the refolding lysozyme is shown in Figure 6. The data fit very well to a single exponential with a rate of around 94 s^{-1} or a time constant of 11 ms. The fitted curve, however, accounts only for a small part of the expected kinetic amplitude based on the measured fluorescence of the free inhibitor and the enzyme-bound complex. Indeed, during the dead time, already 85% of the fluorescence change has been accomplished. This effect clearly shows that native contacts that allow inhibitor binding are already formed during the very early moments of the folding process.

The accomplishment of the fully active state with stable and nonfluctuating native interactions is achieved in an exponential process with a rate of 94 s^{-1}. This value corresponds well with the refolding rate determined by the intrinsic fluorescence of the Trp residues of pigeon lysozyme (Figure 3).

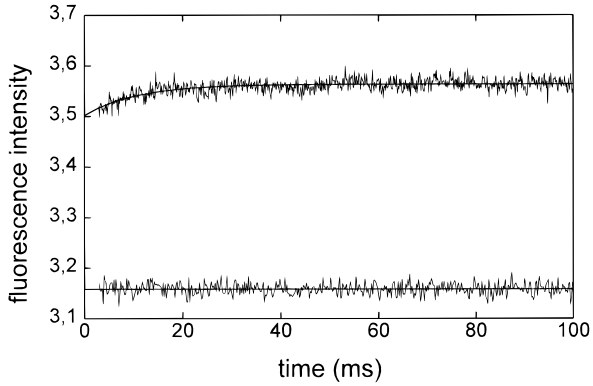

FIGURE 6: Time course of the refolding of pigeon lysozyme in 0.54 M GdnHCl, 20 mM MES, 80 mM NaCl, 2 mM Ca^{2+}, pH 6.0 and 25 °C, monitored by the fluorescence intensity of MeU-diNAG included in the refolding buffer. The lower base line represents the fluorescence of the free MeU-diNAG probe. The upper trace is the fluorescence intensity of the probe during the refolding of pigeon lysozyme and can be fitted by a single exponential (full line). Its asymptote equals the fluorescence intensity of bound MeU-diNAG to the fully native protein.

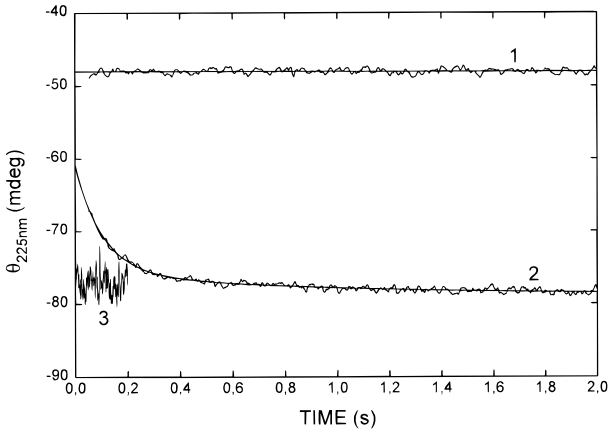

FIGURE 7: Refolding of pigeon lysozyme in 20 mM MES, 80 mM NaCl, 2 mM Ca^{2+}, pH 6.0 and 24.5 °C, monitored by CD at 225 nm. Curve 1 gives the ellipticity in 6 M GdnHCl; curve 2 shows the kinetics in 2 M and curve 3 in 0.54 M GdnHCl.

Refolding Monitored by CD. The refolding kinetic data obtained by far-UV CD are shown in Figure 7. Refolding from 6 to 0.54 M GdnHCl is totally completed within the dead-time of the instrument. Under these conditions, all the native secondary structure has already been formed during the initial burst phase. From our stopped-flow fluorescence measurements, it was demonstrated (Figure 5) that the apparent reaction rate slows down by increasing the final GdnHCl concentration. In a refolding experiment to 2 M GdnHCl, the formation of native secondary structure can be observed in more detail. In that case, the kinetic trace can be fitted to a double exponential function with rates of 9.6 ± 0.3 and 1.2 ± 0.1 s^{-1}, respectively. The fast phase accounts for 82% of the amplitude, the slow phase for the remaining 18%.

DISCUSSION

Equilibrium and Kinetic Intermediates. The kinetic folding pathway, as can be deduced from kinetic stopped-flow experiments, describes the folding mechanism, i.e., the sequence of events that progressively lead to the native state. This kinetic pathway refers to the time-course of the folding

process and the intermediate conformations that become populated to a measurable extent along this path.

To be detected as an independent species in kinetic folding (or unfolding) experiments, an intermediate must occupy a free energy well that is lower than all prior wells in the pathway, and it must be blocked by a barrier that is higher than all previous barriers. Therefore, if there are any intermediates observed, in most kinetic experiments their number is restricted to 1 or 2. If large kinetic barriers are not encountered, the individual partially refolded (or unfolded) states will not be significantly populated, and no intermediate will be detected. If a late barrier does cause an intermediate to accumulate, this intermediate will overrule all the prior ones and will be observed as the only one (*35*, *36*).

The equilibrium pathway, on the other hand, describes the protein conformations that have the highest probability of being populated along a sequence of gradually changing conditions. Equilibrium studies permit identification of the protein conformations that have the lowest energy levels but provide no information on the level of the transition state and the corresponding rate-limiting step. In many instances, it has been shown that kinetic and equilibrium intermediates resemble each other (*3*, *37*−*39*). These observations led to the suggestion that the formation of a compact state with nativelike secondary structure but fluctuating tertiary structure may be a productive intermediate on a more or less direct kinetic route toward the native state (*1*). In other words, a molten globular intermediate state limits the conformational search and directs—on pathway—the polypeptide chain toward the native conformation. This classical view has been challenged by theoretical (*40*) and experimental indications (*6*, *41*) that in some situations conformational states accumulating in kinetic refolding experiments represent misfolded species. In this way, non-native interactions can lead to kinetically trapped states. These intermediates are off pathway and are nonproductive for reaching the native structure.

Pigeon lysozyme shows an equilibrium as well as a kinetic intermediate. Direct proof for the possible identity of both states is hard to furnish as the equilibrium and the kinetic intermediate states appear in totally different conditions. From our CD measurements, it is clear that in pigeon lysozyme both intermediate states possess a high secondary structure content. Some difference in the organization of tertiary structure, however, can be demonstrated. In the kinetic intermediate, the tertiary structure has been developed in a way such that the protein binds the substrate analogue MeU-diNAG. This is a most interesting observation as it shows that during the initial collapse of the protein, a significant amount of native contact is established. Binding of MeU-diNAG to the equilibrium intermediate could not be demonstrated as the use of this probe is not compatible with the low pH required for a sufficient population of the equilibrium intermediate. Analysis of the ellipticity measurements in the near-UV region at 276 nm (Figure 2) indicates that the equilibrium intermediate is characterized by exclusively nonspecific tertiary contacts. This contrasts with the fixed native tertiary contacts present in the kinetic intermediate state as proved by the binding of the substrate analogue.

Effect of Ca^{2+} Binding. Another interesting feature in the folding behavior of pigeon lysozyme is appearing from the Ca^{2+}-binding experiments. The binding of Ca^{2+} does not accelerate the protein folding process, in contrast to what is observed in α-lactalbumin (*25*) and in Ca^{2+}-binding mutants of human lysozyme (Haezebrouck, Noyelle, Joniau, and Van Dael, unpublished results). In all these proteins, pigeon lysozyme included, the stability and the resistance toward thermal and chemical denaturation are strongly enhanced upon Ca^{2+} binding. Our kinetic results for pigeon lysozyme indicate that folding speed and stability do not necessarily increase simultaneously. This conclusion is consistent with that drawn from experiments on the cold-shock protein CspB, which is only marginally stable but folds extremely rapidly (*42*), and on two fragments of the streptococcal G protein, the folding rates of which are inversely related to their stabilities (*43*).

For proteins which have different intrinsic stabilities for the different domain, it is expected that the most stable domain will fold first, inducing a kinetic intermediate with properties resembling the corresponding equilibrium molten globule. In this respect, α-lactalbumin is the best studied and most representative example. The stable α-domain folds first, giving rise to an equilibrium and kinetic intermediate with fluctuating structure in the β-domain. The fully native structure of the protein is only adopted in the presence of a correctly folded β-domain. Besides a significant enhancement of the stability, binding of calcium to α-lactalbumin favors the nativelike fold by breaking up folding barriers associated with non-native interactions. In pigeon lysozyme that intrinsically folds fast, there are presumably less non-native interactions that can hamper rapid folding toward the native state. Reasoning in terms of domains, this suggests that in pigeon lysozyme the interdomain contacts are well-developed, hereby promoting the native state, even in the absence of calcium ions.

Role of Tyr or Trp 62 in the Folding Process of Lysozymes. The refolding of pigeon lysozyme is characterized by the formation of an early intermediate state in which the secondary structural elements possess the native conformation. During the burst phase, a substantial part of native tertiary interactions is also formed as probed by the important fluorescence change during the dead-time. The binding of the substrate analogue to the early intermediate state is additional proof for the presence of fixed native contacts. An early intermediate state (I_1) with different properties has also been observed in kinetic studies of hen egg white lysozyme monitored by various techniques such as near- and far-UV CD, absorbance, fluorescence, inhibitor and bis-ANS binding, and H/D exchange detected by mass spectroscopy and NMR (*33*, *44*−*48*). In hen lysozyme, I_1 is succeeded in a sequential model by a second intermediate, I_2, that is stabilized by non-native tertiary interactions (*47*, *49*). The most striking experimental evidence for the presence of this state is the observation of its far-UV ellipticity, that is considerably more negative than the corresponding ellipticity of native lysozyme. The Trp fluorescence of this state is very highly quenched (*33*, *47*), which suggested that during the refolding process Trp 62 and/or Trp 108 are involved in non-native tertiary interactions. Refolding studies on two mutants of hen lysozyme in which Trp 62 and Trp 108 have been individually replaced by tyrosine residues (*49*) have

shown that the intermediate I_2 does not appear and that both these mutants fold significantly faster than wild-type lysozyme. These authors therefore conclude that the rate-limiting step in the folding of hen lysozyme does not arise from any inherent slowness in the formation of the native structure but rather as a consequence of the formation of a highly stable intermediate which contains significant non-native structure. Prior to subsequent folding or in concert with that folding, this non-native structure has to be disrupted. Like hen lysozyme, pigeon lysozyme possesses Trp residues at positions 28, 63, 108, and 111. At positions 62 and 123, however, the Trp residues of hen lysozyme are substituted for Tyr in the pigeon variant. It is remarkable that in pigeon lysozyme the I_2 state, described for wild-type hen lysozyme and characterized by the corresponding negative overshoot of the fluorescence signal, is not observed even not after varying the final GdnHCl concentration. Concomitant with this observation, pigeon lysozyme folds markedly faster than hen egg white lysozyme does. The fully native state is accomplished with a rate constant of 135 s^{-1} (Table 1) for pigeon lysozyme compared with rate constants of 2.9 s^{-1} (*33*), 2.2 s^{-1} (*47*), and 2.6 s^{-1} (*6*) for hen lysozyme in slightly different buffer conditions. Very recently, it has been shown that besides folding through an intermediate state, hen lysozyme directly folds through a fast direct pathway with a rate constant of about 25 s^{-1} (*50*). This is still significantly slower than the folding rate that we observed for pigeon lysozyme. Our results on pigeon lysozyme are in complete agreement with those obtained on the Tyr mutants of hen lysozyme (*49*), as well for the nonappearance of I_2 as for the high rate constant. All this leads to the conclusion that Trp 62 stabilizes the I_2 state presumably by participating in non-native tertiary interactions. It should be noted here that the refolding of wild-type human lysozyme, which also has Tyr residues at positions 62 and 124 (corresponding with 123 in hen and pigeon lysozyme), similarly does not exhibit the unusual fluorescence or ellipticity behavior of hen lysozyme and proceeds about 4 times more rapidly (*51*). Although the possible role of other residues (e.g., Trp 123) is not systematically explored yet, it is clear that Trp 62 is crucial in stabilizing nonproductive interactions for folding. Its replacement by Tyr in pigeon lysozyme enhances the formation of native tertiary contacts. Recent investigations of Lu et al. (*52*) on the folding behavior of hen lysozyme have shown that the slow step in its refolding is associated primarily with the reorganization of hydrophobic interactions. Presumably in pigeon lysozyme Tyr 62 facilitates the right hydrophobic contacts that direct the molecule toward the native state.

Energy Profile of the Folding−Unfolding Transition. A free energy diagram (Figure 8) can be deduced from the kinetic parameters combined with the equilibrium unfolding data. The activation free energy change to the transition state in water $\Delta G^{\#}(H_2O)$, can be calculated from the rate constant in water, $k(H_2O)$, by Eyring's equation 53:

$$\Delta G^{\#}(H_2O) = RT \ln [k_B T/hk(H_2O)] \qquad (8)$$

where k_B and h are the Boltzmann and Planck constants, respectively.

Here, we have determined the activation energy for unfolding from native to unfolded state $\Delta G^{\#}_{unf}(H_2O) = 83.6 \pm 0.5$ kJ mol^{-1}, and the activation energy for refolding from burst-phase intermediate to native state, $\Delta G^{\#}_{ref}(H_2O) = 59.3 \pm 0.5$ kJ mol^{-1}, based on $k_{NU}(H_2O)$ and $k_{IN}(H_2O)$, respectively.

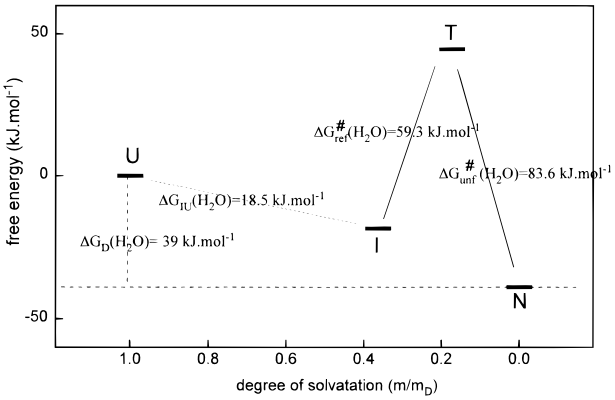

FIGURE 8: Gibbs energy profile for the different states in the folding pathway of pigeon egg white lysozyme in water. $\Delta G^{\#}_{unf}(H_2O)$ and $\Delta G^{\#}_{ref}(H_2O)$ indicate the activation free energies for the unfolding and refolding, respectively. $\Delta G_D(H_2O)$ and $\Delta G_{IU}(H_2O)$ represent the free energy differences between the native and unfolded states and between the intermediate and unfolded states, respectively. Free energy values from the ordinate are expressed in a relative way to the free energy of the unfolded state and are plotted using the degree of solvatation as a reaction coordinate. Because there is no information about the rate of the reaction from U to I, this transition is shown as a broken line.

Values for $m^{\#}_{ref}$ and $m^{\#}_{unf}$ can be calculated directly from the slopes of the V-shaped curve of the kinetic experiments (*54*). The kinetic parameters m_{NU} and m_{IN} were multiplied by a factor $-2.3026RT$ for comparison with equilibrium m values derived from unfolding curves: $m^{\#}_{unf} = (-2.3026RT)m_{NU}$ and $m^{\#}_{ref} = (-2.3026RT)m_{IN}$. We have obtained $m^{\#}_{unf} = -2.1 \pm 0.1$ kJ mol^{-1} M^{-1} and $m^{\#}_{ref} = 2.3 \pm 0.6$ kJ mol^{-1} M^{-1}. The m values for particular states are a measure of their relative solvent exposure or compactness. The degree of solvatation therefore can be used as a reaction coordinate for the folding−unfolding process and has been plotted against the free energy in Figure 8 (*9*). The degree of solvatation associated with each state was calculated as a fraction of the total change observed during the N ↔ U transition.

The free energy profile indicates the following relations:

$$\Delta G_{NI}(H_2O) = \Delta G_D(H_2O) - \Delta G_{IU}(H_2O) \qquad (9)$$

$$\Delta G_{NI}(H_2O) = \Delta G^{\#}_{unf}(H_2O) - \Delta G^{\#}_{ref}(H_2O) \qquad (10)$$

$\Delta G_{NI}(H_2O)$ can thus be obtained in two different ways, namely, based on unfolding curves (eq 9) or from rate constants (eq 10). Both values 21 ± 2 kJ mol^{-1} (eq 9) and 24 ± 1 kJ mol^{-1} (eq 10) coincide well with each other within experimental error, indicating that the energy profile presented in Figure 8 is very plausible.

Similarly, a value for m_{NI} can be calculated from equilibrium m values (eq 11) or from kinetically determined parameters (eq 12).

$$m_{NI} = m_D - m_{IU} \qquad (11)$$

$$m_{NI} = m^{\#}_{unf} - m^{\#}_{ref} \qquad (12)$$

Again, both values, -5.5 ± 0.7 kJ mol^{-1} M^{-1} (eq 11) and -4.4 ± 0.7 kJ mol^{-1} M^{-1} (eq 12), are equal within error limits.

The kinetic folding intermediate, that is evident from our experiments, lies directly on the pathway between U and N, supporting the sequential model U → I → N. This refolding intermediate is shown to be more stable than the denaturant-induced unfolded state by 18.5 kJ mol^{-1} under physiological conditions. Therefore, rather than the unfolded state, the refolding intermediate is the latent denatured state under physiological conditions. Figure 8 also reveals an important reduction of the degree of solvatation by going from the unfolded state to the early intermediate state. The formation of this kinetic intermediate is thus accompanied by a major collapse. A supplementary decrease in solvent-exposed surface is observed when the unfolding proceeds by a further I → N transition.

Taken together, we can conclude that pigeon lysozyme is an extremely rapid folding protein. The observed kinetic intermediate is on pathway, does not stabilize non-native interactions, and is efficient for further folding. Binding of Ca^{2+} ions that obviously increase the protein stability does not affect the folding speed. Study of the energetics of the folding process shows that the intermediate is located between the unfolded state and the native state on a linear reaction pathway.

ACKNOWLEDGMENT

Expert technical assistance was provided by W. Noppe and S. Vanryckeghem. We thank Prof. M. Joniau for his critical reading of the manuscript.

REFERENCES

1. Roder, H. (1995) *Nat. Struct. Biol. 2*, 817−820.
2. Ptitsyn, O. B. (1995) *Adv. Protein Chem. 47*, 83−229.
3. Colon, W., and Roder, H. (1996) *Nat. Struct. Biol. 3*, 1019−1025.
4. Miranker, A., and Dobson, C. M. (1996) *Curr. Opin. Struct. Biol. 6*, 31−42.
5. Baldwin, R. L. (1995) *J. Biomol. NMR 5*, 103−109.
6. Kiefhaber, T. (1995) *Proc. Natl. Acad. Sci. U.S.A. 92*, 9029−9033.
7. Baldwin, R. L. (1996) *Folding Des. 1*, R1−R8.
8. Matouschek, A., Kellis, J. T., Jr., Serrano, L., Bycroft, M., and Fersht, A. R. (1990) *Nature 346*, 440−445.
9. Parker, M. J., Spencer, J., and Clarke, A. R. (1995) *J. Mol. Biol. 253*, 771−786.
10. Sauder, J. M., MacKenzie, N. E., and Roder, H. (1996) *Biochemistry 35*, 16852−16862.
11. Rodriguez, R., Menendez-Arias, L., Gonzalez de Buitrago, G., and Gavilanes, J. G. (1985) *Biochem. Int. 11*, 841−843.
12. Nitta, K., Tsuge, H., Shimazaki, K., and Sugai, S. (1988) *Biol. Chem. Hoppe-Seyler 369*, 671−675.
13. Yao, M., Tanaka, I., Hikichi, K., and Nitta, K. (1992) *J. Biochem. 111*, 1−3.
14. Acharya, K. R., Stuart, D. I., Phillips, D. C., McKenzie, H. A., and Teahan, C. G. (1994) *J. Protein Chem. 13*, 569−584.
15. Nitta, K., Tsuge, H., and Iwamoto, H. (1993) *Int. J. Pept. Protein Res. 41*, 118−123.
16. Van Dael, H., Haezebrouck, P., Morozova, L., Arico-Muendel, C., and Dobson, C. (1993) *Biochemistry 32*, 11886−11894.
17. Griko, Y. V., Freire, E., Privalov, G., Van Dael, H., and Privalov, P. L. (1995) *J. Mol. Biol. 252*, 447−459.
18. Morozova, L. A., Haynie, D. T., Arico-Muendel, C., Van Dael, H., and Dobson, C. M. (1995) *Nat. Struct. Biol. 2*, 871−875.
19. Haezebrouck, P., Joniau, M., Van Dael, H., Hooke, S. D., Woodruff, N. D., and Dobson, C. M. (1995) *J. Mol. Biol. 246*, 382−387.
20. Babu, K. R., and Bhakuni, V. (1997) *Eur. J. Biochem. 245*, 781−789.
21. Noppe, W., Hanssens, I., and De Cuyper, M. (1996) *J. Chromatogr. A719*, 327−331.
22. Gavilanes, J., González de Buitrago, G., Martinez del Pozo, A., Pérez-Castells, R., and Rodríguez, R. (1982) *Int. J. Pept. Protein Res. 20*, 238−245.
23. Nozaki, Y. (1972) *Methods Enzymol. 26*, 43−50.
24. Griko, Y. V., Freire, E., and Privalov, P. L. (1994) *Biochemistry 33*, 1889−1899.
25. Kuwajima, K., Mitani, M., and Sugai, S. (1989) *J. Mol. Biol. 206*, 547−561.
26. Khorasanizadeh, S., Peters, I. D., Butt, T. R., and Roder, H. (1993) *Biochemistry 32*, 7054−7063.
27. Sendak, R. A., Rothwarf, D. M., Wedemeyer, W. J., Houry, W. A., and Scheraga, H. A. (1996) *Biochemistry 35*, 12978−12992.
28. Pace, C. N. (1975) *CRC Crit. Rev. Biochem. 3*, 1−43.
29. Santaro, M. M., and Bolen, D. W. (1988) *Biochemistry 27*, 8063−8068.
30. Yamasaki, K., Ogasahara, K., Yutani, K., Oobatake, M., and Kanaya, S. (1995) *Biochemistry 34*, 16552−16562.
31. Khorasanizadeh, S., Peters, I. D., and Roder, H. (1996) *Nat. Struct. Biol. 3*, 193−205.
32. Yang, Y., and Hamaguchi, K. (1980) *J. Biochem. 87*, 1003−1014.
33. Itzhaki, L. S., Evans, P. A., Dobson, C. M., and Radford, S. E. (1994) *Biochemistry 33*, 5212−5220.
34. Kotik, M., Radford, S. E., and Dobson, C. M. (1995) *Biochemistry 34*, 1714−1724.
35. Bai, Y., and Englander, W. (1996) *Proteins: Struct., Funct., Genet. 24*, 145−151.
36. Hilser, V. J., and Freire, E. (1996) *J. Mol. Biol. 262*, 756−772.
37. Hughson, F. M., Wright, P. E., and Baldwin, R. L. (1990) *Science 249*, 1544−1548.
38. Jennings, P. A., and Wright, P. E. (1993) *Science 262*, 892−895.
39. Balbach, J., Forge, V., Van Nuland, N., Winder, S., Hore, P., and Dobson, C. M. (1995) *Nat. Struct. Biol. 2*, 865−870.
40. Wolynes, P. G., Onuchic, J. N., and Thirumalai, D. (1995) *Science 267*, 1619−1620.
41. Sosnick, T. R., Mayne, L., Hiller, R., and Englander, S. W. (1994) *Nat. Struct. Biol. 1*, 149−156.
42. Schindler, T., Herrler, M., Marahiel, M. A., and Schmid, F. X. (1995) *Nat. Struct. Biol. 2*, 633−673.
43. Alexander, P., Orban, J., and Bryan, P. (1992) *Biochemistry 31*, 7243−7248.
44. Chafotte, A. F., Guillon, Y., and Goldberg, M. E. (1992) *Biochemistry 31*, 9694−9702.
45. Radford, S. E., Dobson, C. M., and Evans, P. A. (1992) *Nature 358*, 302−307.
46. Miranker, A., Robinson, C. V., Radford, S. E., Aplin, R. T., and Dobson, C. M. (1993) *Science 262*, 896−900.
47. Denton, M. E., Rothwarf, D. M., and Sheraga, H. A. (1994) *Biochemistry 33*, 11225−11236.
48. Hooke, S. D., Eyles, S. J., Miranker, A., Radford, S. E., Robinson, C. V., and Dobson, C. M. (1995) *J. Am. Chem. Soc. 117*, 7548−7549.
49. Rothwarf, D. M., and Sheraga, H. A. (1996) *Biochemistry 35*, 13797−13807.
50. Wildegger, G., and Kiefhaber, T. (1997) *J. Mol. Biol. 270*, 294−304.
51. Hooke, S. D., Radford, S. E., and Dobson, C. M. (1994) *Biochemistry 33*, 5867−5876.
52. Lu, H., Buck, M., Radford, S. E., and Dobson, C. M. (1997) *J. Mol. Biol. 265*, 112−117.
53. Eyring, H. (1935) *Chem. Phys. Rev. 17*, 65−77.
54. Sosnick, T. R., Mayne, L., and Englander, S. W. (1996) *Proteins: Struct., Funct., Genet. 24*, 413−426.

BI973105W